Mutations in the Putative H-Channel in the Cytochrome *c* Oxidase from *Rhodobacter sphaeroides* Show That This Channel Is Not Important for Proton Conduction but Reveal Modulation of the Properties of Heme *a*†

Hang-mo Lee,‡ Tapan Kanti Das,§ Denis L. Rousseau,§ Denise Mills,|| Shelagh Ferguson-Miller,|| and Robert B. Gennis*,‡

Departments of Chemistry and Biochemistry, University of Illinois, Urbana, Illinois 61801, Department of Physiology and Biophysics, Albert Einstein College of Medicine, Bronx, New York 10461, and Department of Biochemistry, Michigan State University, East Lansing, Michigan 48824

Received October 26, 1999; Revised Manuscript Received January 3, 2000

ABSTRACT: As the final electron acceptor in the respiratory chain of eukaryotic and many prokaryotic organisms, cytochrome *c* oxidase catalyzes the reduction of oxygen to water, concomitantly generating a proton gradient. X-ray structures of two cytochrome *c* oxidases have been reported, and in each structure three possible pathways for proton translocation are indicated: the D-, K-, and H-channels. The putative H-channel is most clearly delineated in the bovine heart oxidase and has been proposed to be functionally important for the translocation of pumped protons in the mammalian oxidase [Yoshikawa et al. (1998) *Science 280*, 1723−1729]. In the present work, the functional importance of residues lining the putative H-channel in the oxidase from *Rhodobacter sphaeroides* are examined by site-directed mutagenesis. Mutants were generated in eight different sites and the enzymes have been purified and characterized. The results suggest that the H-channel is not functionally important in the prokaryotic oxidase, in agreement with the conclusion from previous work with the oxidase from *Paracoccus denitrificans* [Pfitzner et al. (1998) *J. Biomembr. Bioenerg. 30*, 89−93]. Each of the mutants in *R. sphaeroides*, with an exception at only one position, is enzymatically active and pumps protons in reconstituted proteoliposomes. This includes H456A, where in the *P. denitrificans* oxidase a leucine residue substituted for the corresponding residue resulted in inactive enzyme. The only mutations that result in completely inactive enzyme in the set examined in the *R. sphaeroides* oxidase are in R52, a residue that, along with Q471, appears to be hydrogen-bonded to the formyl group of heme *a* in the X-ray structures. To characterize the interactions between this residue and the heme group, resonance Raman spectra of the R52 mutants were obtained. The frequency of the heme *a* formyl stretching mode in the R52A mutant is characteristic of that seen in non-hydrogen-bonded model heme *a* complexes. Thus the data confirm the presence of hydrogen bonding between the heme *a* formyl group and the R52 side chain, as suggested from crystallographic data. In the R52K mutant, this hydrogen bonding is maintained by the lysine residue, and this mutant enzyme retains near wild-type activity. The heme *a* formyl frequency is also affected by mutation of Q471, confirming the X-ray models that show this residue also has hydrogen-bonding interactions with the formyl group. Unlike R52, however, Q471 does not appear to be critical for the enzyme function.

Cytochrome *c* oxidase is a key enzyme in aerobic metabolism. It catalyzes the reduction by cytochrome *c* of dioxygen to water, utilizing the exergonic reaction to translocate protons against a gradient. Cytochrome *c* oxidase belongs to the superfamily of heme-copper respiratory oxidases that are thought to share common mechanisms for dioxygen reduction and proton pumping (*1*−*4*). The structural similarity in the main subunits of the cytochrome *c* oxidases from the reported structures of eukaryotic (bovine heart mitochondria) and prokaryotic (*Paracoccus denitrificans*) oxidases support this view (*2*, *5*, *6*).

Cytochrome *c* oxidase contains four metal redox cofactors. Heme a_3 and Cu_B comprise the binuclear center, the active site of the enzyme where the reduction of dioxygen to water occurs. Electrons derived from cytochrome *c* are delivered to the binuclear center by sequential electron transfer, first to Cu_A, then to heme *a*, and finally to the heme a_3−Cu_B binuclear center (*2*, *5*, *6*). For each molecule of dioxygen that is reduced, four protons are taken from the "inside" aqueous phase (electronegative) for the generation of water at the active site, and another four protons are pumped across the membrane.

$$\mathbf{8\ H_{in}}^{+} + 4\ \text{cyt}\ c^{2+} + O_2 \rightleftharpoons 4\ \text{cyt}\ c^{3+} + 2\ H_2O + \mathbf{4\ H_{out}}^{+}$$

† Supported by grants from the National Institutes of Health HL16101 (to R.B.G.), GM54806 and GM54812 (to D.L.R.), and GM26916 and NIH Fellowship F32GM18206 (to DM).

* Corresponding author: Department of Biochemistry, University of Illinois, 600 S. Mathews St., Urbana, IL 61801. Tel 217-333-9075; FAX 217-244-3186; Email r-gennis@uiuc.edu.

‡ University of Illinois.

§ Albert Einstein College of Medicine.

|| Michigan State University.

10.1021/bi9924821 CCC: $19.00
Published on Web 02/25/2000

The "chemical" or substrate protons traverse approximately 30 Å through the protein to reach the binuclear center, and the pumped protons are translocated by approximately 50 Å (*5*−*7*). Pathways must be present within the protein to facilitate the proton translocation through the protein (*8*). In the X-ray structures three possible proton-conducting pathways have been identified and named according to conserved amino acid residues: the D-, K-, and H-channels (*6*, *9*, *10*). Key residues within the D-channel and K-channel have been shown by site-directed mutagenesis to be functionally important (*7*, *8*). The D-channel begins at D132 (*Rhodobacter sphaeroides* numbering), near the surface of the protein, and clearly provides a hydrogen-bond network with numerous internal water molecules that leads to E286 (*R. sphaeroides* numbering), which is about 10 Å away from the heme−copper center. The proton pathway beyond E286 is not evident from the static structure, and it is possible that both pumped as well as chemical protons are translocated through this channel to E286 (*8*). Mutagenesis data provide a strong case that the D-channel is critical to deliver protons for the oxygen chemistry following the binding of dioxygen and also is a critical component of the conduit for pumped protons. Some mutants in the D-channel have severely reduced enzymatic activity and the residual activity is decoupled from proton pumping (*11*, *12*). Mutations within the K-channel (e.g., K362M in the *R. sphaeroides* oxidase) also have a deleterious effect on the enzyme, primarily by blocking proton delivery to the active site that is necessary to reduce the heme−copper center prior to the binding of dioxygen (*12*, *13*).

The presence of the third putative proton-conducting H-channel was first suggested by the bovine crystal structure (*6*, *9*) and later also identified in the *P. denitrificans* (*10*) structure. This putative channel, named for a partially conserved histidine found in the channel (*14*) (H456 in the *R. sphaeroides* oxidase), has been delineated all the way across the membrane and has been proposed to be specifically utilized to convey pumped protons in the mammalian oxidases. Note that the pathway of the H-channel does not lead to the heme−copper binuclear center but, instead, comes in contact with heme *a*. The putative channel has a hydrogen-bond network starting with residue D407 (bovine numbering) on the electronegative side of the membrane and continues through H413, T424, S461, S382, heme *a*, S454, Q428, R38, N451, and Y443 on the electropositive side of the membrane (*6*). The putative channel was later modified to go from N451 to Y371, heme *a* (propionate), Y54, amide backbone (441/440), and then D51, which is near the interface with subunit II and the Cu_A site (*9*). It was demonstrated that the conformation of the bovine oxidase changed upon oxidation and reduction, resulting in changes in the access of D51 to the bulk solvent and, thus, providing a rationale for how this structure might function as a channel whose conductance is dependent on the redox state of the enzyme (*9*). The connectivity with heme *a* is observed at (1) residue S382 (bovine numbering), which is hydrogen-bonded to the hydroxyl moiety on the hydroxyethyl farnesyl side chain of heme *a*; (2) residues R38 and Q428, which are hydrogen-bonded to the formyl group of heme *a* (*5*, *9*); and (3) residues Y371 and Y54 which are both hydrogen-bonded to one of the propionate groups of heme *a* (*9*).

In this work, mutations are reported in eight residues of the *R. sphaeroides* oxidase that correspond to residues identified in the structure of the bovine heart oxidase as lining the putative H-channel. The mutant enzymes are isolated and characterized. In all but one case, the enzymes retain catalytic activity that is coupled to proton pumping similar to that of the wild-type enzyme. The one exception is the R52A mutant, a nonconservative substitution in the residue corresponding to R38 in the bovine oxidase. As predicted by the X-ray structural models of the enzyme, this mutant is grossly perturbed spectroscopically in a manner consistent with the elimination of a hydrogen bond to the formyl group of heme *a*. The R52A mutant is also enzymatically inactive.

MATERIALS AND METHODS

Materials. All chemicals used were of reagent grade. Dodecyl β-D-maltoside was obtained from Anatrace. Ni^{2+}−NTA agarose was obtained from Qiagen. CCCP, valinomycin, ferricyanide, dithionite, and horse heart cytochrome *c* (type VI) were from Sigma. DNA oligonucleotides were synthesized by the University of Illinois Biotechnology Center (Urbana, IL) or by Operon Technologies, Inc. Vent (exo^-) polymerase for PCR was obtained from New England Biolabs. *Pfu* polymerase for PCR and QuickChange site-directed mutagenesis kits were obtained from Strategene. Restriction enzymes were obtained from New England Biolabs and Gibco−BRL.

Site-Directed Mutagenesis. Site-directed mutants were constructed by three separate methods. S425A, T467V, and Q471A were constructed by extension of a single mutagenic oligonucleotide (*15*). E450L was constructed by the two-step PCR method descirbed by Landt et al. (*16*). R52A, R52K, R52Q, H456A, and S504A were constructed with QuickChange site-directed mutagenesis kits (Strategene). Y414F was His-tagged by replacing the DNA fragment of *Hind*III and *Sph*I with the corresponding pJS3(X6H) fragment, which contained DNA coding for six histidines at the C-terminus (*17*). All mutations were verified by DNA sequencing and checked for any mistakes that might have occurred elsewhere during the PCR or amplification.

Protein Preparation. Wild-type and mutant cytochrome *c* oxidase, modified by a six-histidine affinity tag, were purified from *R. sphaeroides* as described previously (*17*). The protein concentration was determined with a BCA kit (Pierce) or by UV/vis spectroscopy as described previously (*17*).

Activity Assay. Activity was monitored spectrophotometrically by following oxidation of ferrocytochrome *c* at 550 nm with a Shimadzu UV-2101PC instrument. Reaction conditions were as follows: 50 mM potassium phosphate, pH 6.5, 0.02% dodecyl β-D-maltoside, and 2−50 μM ferrocytochrome *c*.

Proton Pumping Measurement. Reconstitution of cytochrome *c* oxidase was carried out as published (*18*) with the following modifications. Concentrated cytochrome *c* oxidase was diluted into 75 mM HEPES−KOH with 4% cholate prior to the addition of an equal volume of 40 mg/mL purified asolectin lipids in 2% cholate and 75 mM HEPES−KOH, pH 7.4. The mixture was sonicated and centrifuged to give a final concentration of 2 μM oxidase and 20 mg/mL lipids. Successive dialysis was used to remove detergent.

The vesicles were dialyzed into a final buffer of 50 mM HEPES−KOH, pH 7.4, 45 mM KCl, and 44 mM sucrose. Concentrated cytochrome *c* was prereduced with sodium dithionite and desalted through a Sephadex G-75 column. Proton pumping was measured by use of an Online Systems rapid-scanning monochromator stopped-flow instrument with a 0.4 cm cuvette. Final concentrations were 80 nM cytochrome *c* oxidase (vesicles), 2−5 μM ferrocytochrome *c*, and 100 μM phenol red. Multiple shots were taken for each sample and averaged before generating the difference spectra (reduced−oxidized). Kinetic traces were taken at the isosbestic point for cytochrome *c* (556.8 nm) to monitor the changes in the spectrum of phenol red: under coupled conditions, in the presence of 2 μM valinomycin, and with 2 μM valinomycin and 5 μM CCCP present. Because of an early slight acidification that is an artifact of the system, the kinetic trace (at 556.8 nm) obtained under the coupled conditions was subtracted from that in which the enzyme was uncoupled by valinomycin. Additionally, after correcting for back-leak, the coupled trace was subtracted from the uncoupled trace. Stoichiometry of the proton pumping (H_T^+/e^-) can be calculated from the Δ(absorbance) of the uncoupled enzyme, assuming 1 substrate proton is used per electron (H_S^+/e^-). The rates of cytochrome *c* oxidation were analyzed by global analysis using a first-order fit, and the rates of changes in the spectrum of phenol red were calculated with Microcal Origin software.

Respiratory Control. The oxygen consumption of the reconstituted cytochrome *c* oxidase was measured polarographically as before (*12*) under coupled conditions, after addition of 1.2 μM valinomycin, and with the addition of 5.9 μM CCCP for the uncoupled activity.

Resonance Raman Measurements. The Raman experiments were carried out with 441.6 nm excitation from a CW He−Cd laser (Liconix, Santa Clara, CA) and with 413.1 nm excitation from a CW Kr ion laser (Spectra Physics, Mountain View, CA). The sample cell (quartz, 2 mm path length, sample volume ~150 μL) into which a laser beam was focused, was spun at 3000−6000 rpm to minimize local heating. The sample cells are custom-designed for strict anaerobic measurements and can be used for recording both the resonance Raman spectra and the optical absorption spectra (UV-2100U spectrophotometer, Shimadzu, Kyoto, Japan). The Raman scattered light was focused onto the entrance slit (100 μm) of a polychromator (Spex, Metuchen, NJ), dispersed by a 1200 grooves/mm grating and detected by a high-performance liquid nitrogen-cooled charged-couple device (CCD) (Princeton Instruments, Trenton, NJ). Cooling of the CCD to low temperature dramatically diminishes the dark count, thereby allowing a long period of data acquisition when necessary. A holographic notch filter (Kaiser, Ann Arbor, MI) was used to eliminate Rayleigh scattering. Typically, several 30 s spectra were recorded and averaged. Frequency shifts in the Raman spectra were calibrated with acetone−CCl_4 (for the 100−1000 cm^{-1} region) and indene (for the 100−1700 cm^{-1} region) as references. The accuracy of the Raman shifts is about $\pm$2 cm^{-1} for absolute shifts and about $\pm$0.5 cm^{-1} for relative shifts. The Raman spectra were processed by using GRAMS (Galactic Industries Corp.) software. The cosmic ray spikes were removed by using CSMA subroutines (Princeton Instruments). In a few cases, simple background corrections were employed, but the spectra were not smoothed.

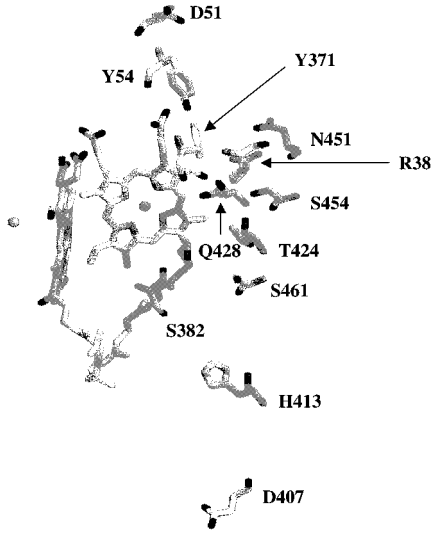

FIGURE 1: Proposed H-channel residues found in bovine heart mitochondrial cytochrome *c* oxidase. Aspartate 407 is at the entrance of the channel near the negative side, and aspartate 51 is near the electropositive side where protons may exit. Cu_B and heme a_3 are also shown. The amide backbone of 440/441 located between D51 and Y54 is not shown. Oxygen atoms are black and nitrogen atoms are darker gray. The residues are numbered according to the bovine sequence. The X-ray structure coordinates used are 2OCC of bovine heart mitochondrial cytochrome *c* oxidase and the figure is prepared with RASMOL.

The concentration of the protein samples used for the Raman measurements was ~15 μM in 100 mM phosphate buffer, pH 7.4. Reduction of the oxidase samples was carried out by injecting buffered dithionite solution in the Raman cell under anaerobic conditions.

RESULTS

Activity and Proton Pumping. The residues lining the putative H-channel of bovine cytochrome *c* oxidase are shown in Figure 1. Residue D407 (bovine numbering; E450 in *R. sphaeroides*) faces the negative side and D51 (bovine numbering; no *R. sphaeroides* equivalent) faces the positive side. Sequence alignments for the homologous oxidases from bovine, *R. sphaeroides*, *P. denitrificans*, and *Escherichia coli* are shown in Figure 2, with the putative H-channel residues highlighted. As can be seen from Figure 2, the oxidase from *E. coli* (cytochrome bo_3 ubiquinol oxidase) does not contain many of the putative H-channel residues, although the enzyme does pump protons (*19*, *20*). The aa_3-type cytochrome *c* oxidases from both *R. sphaeroides* and *P. denitrificans*, however, each contain many of the channel residues found in bovine cytochrome *c* oxidase, with the notable exceptions of residues D51 and Y54 (bovine numbering) near the positive side. The region near D51 is not well conserved in any of the prokaryotic systems but is well conserved among the mammalian oxidases (*9*).

Many of the residues proposed to be lining the putative H-channel (all located in subunit I) in the bovine oxidase have been mutated in the homologous *R. sphaeroides* cytochrome *c* oxidase (Table 1). The mutations were constructed in order to eliminate hydrogen-bonding capabilities of residues in question. With the exception of R52A, all

```
                    15                  30                  45                  60                  75                  90
1 Bovine ---------------  ---------------  -----------MFIN R-WLFSTNHKDIGTL YLLFGAWAGMVGTAL SLLIRAELGQP----      44
2 R.sph  ---------------  ----------MADAA IHGH--EHDRRGFFT R-WFMSTNHKDIGVL YLFTGGLVGLISVAF TVYMRMELMAPGVQF      62
3 P.d.   ---------------  ----------MADAA VHGHGDHHDTRGFFT R-WFMSTNHKDIGIL YLFTAGIVGLISVCF TVYMRMELQHPGVQY      64
4 E.coli MFGKLSLDAVPFHEP IVMVTIAGIILGGLA LVGLITYFGKWTYLW KEWLTSVDHKRLGIM YIIVAIVMLLRGFAD AIMMRSQQALAS---      87

                   105                 120                 135                 150                 165                 180
1 Bovine ----GT---LLG---  -----------DD--  QIYNVVVTAHAFVMI FFMVMPIMIGGFGNW LVPLMIGAPDMAFPR MNNMSFWLLPPSFLL     111
2 R.sph  MCAEHLESGLVKGFF  QSLWPSAVENCTPNG HLWNVMITGHGILMM FFVVIPALFGGFGNY FMPLHIGAPDMAFPR MNNLSYWLYVAGTSL     152
3 P.d.   MCLEGAR--LIA---  -----DASAECTPNG HLWNVMITYHGVLMM FFVVIPALFGGFGNY FMPLHIGAPDMAFPR LNNLSYWMYVCGVAL     144
4 E.coli ----AGEAGFLP---  ------------P--  HHYDQIFTAHGVIMI FFVAMPFVIG-LMNL VVPLQIGARDVAFPF LNNLSFWFTVVGVIL     155

                   375                 390                 405                 420                 435                 450
1 Bovine VWAHHMFTVGMDVDT RAYFTSATMIIAIPT GVKVFSWLATLHGGN IKWSPAMMWALGFIF LFTVGGLTGIVLANS SLDIVLHDTYYVVAH     376
2 R.sph  VWAHHMYTAGLSLTQ QSYFMMATMVIAVPT GIKIFSWIATMWGGS IELKTPMLWALGFLF LFTVGGVTGIVLSQA SVDRYYHDTYYVVAH     419
3 P.d.   VWAHHMYTAGMSLTQ QAYFMLATMTIAVPT GIKVFSWIATMWGGS IEFKTPMLWAFGFLF LFTVGGVTGVVLSQA PLDRVYHDTYYVVAH     411
4 E.coli VWLHHFFTMGAGANV NAFFGITTMIIAIPT GVKIFNWLFTMYQGR IVFHSAMLWTIGFIV TFSVGGMTGVLLAVP GADFVLHNSLFLIAH     419

                   465                 480                 495                 510                 525                 540
1 Bovine FHYVLSMGAVFAIMG GFVHWFPLFSGYTLN DTWAKIHFAIMFVGV NMTFFPQHFLGLSGM PRRYSDYPD-AYTMW NTISSMGSFISLTAV     465
2 R.sph  FHYVMSLGAVFGIFA GSTSGIGKMSGRQYP EWAGKLHFWMMFVGA NLIFFPQHFLGRQGM PRRYIDYPE-AFATW NFVSSLGAFLSFASF     508
3 P.d.   FHYVMSLGAVFGIFA GVYYWIGKMSGRQYP EWAGQLHFWMMFIGS NLIFFPQHFLGRQGM PRRYIDYPV-EFAYW NNISSIGAYISFASF     500
4 E.coli FHNVITGGVVFGCFA GMTYWWPKAFGFKLN ETWGKRAFWFWIIGF FVAFMPLYALGFMGM TRRLSQQIDPQFHTM LMIAASGAVLIALGI     509
```

FIGURE 2: Sequence alignment of some representative oxidases. Shaded boxes indicate residues for the putative H-channel. (1) Bovine heart mitochondria (aa_3 type); (2) *Rhodobacter sphaeroides* (prokaryotic aa_3 type); (3) *Paracoccus denitrificans* (prokaryotic aa_3 type); (4) *Escherichia coli* (prokaryotic bo_3 type). The alignment was done with ClustalW 1.7 found at http://dot.imgen.bcm.tmc.edu:93331/multi-align/multi-aligh.html.

Table 1. Wild-type and Mutant Cytochrome *c* Oxidase Turnover Rate

R. sphaeroides numbering	bovine numbering	turnover rate (e^-/s)
WT		1500
S504A	S461	1570
Q471A	Q428	1200
T467V	T424	1600
H456A	H413	1570
E450L	D407	1300
S425A	S382	1000
Y414F	Y371	800
R52A	R38	Inactive
R52K	R38	980
R52Q	R38	Inactive

[a] Enzyme turnover rate was measured spectroscopically following the oxidation of reduced cytochrome *c* at 550 nm in 50 mM potassium phosphate, pH 6.5, with 0.02% dodecyl maltoside (w/v) at 25 °C.

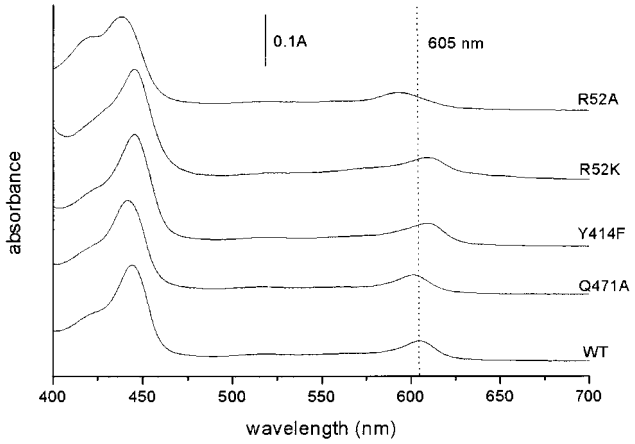

FIGURE 3: UV−Visible spectra of dithionite-reduced wild-type and mutants. The sample buffer consisted of 50 mM potassium phosphate, pH 8.0, and 0.05% (w/v) dodecyl maltoside. Reduced spectra were taken after incubation of the samples with dithionite for 5 min (or until no appreciable difference was found in subsequent measurements). λ_{max} for WT are 605 and 444 nm. λ_{max} for Q471A are 601 and 441.6 nm. λ_{max} for Y414F are 609.4 and 445.4 nm. λ_{max} for R52K are 609.0 and 445.6 nm. λ_{max} for R52A are 592.2, 421.4, and 438.4 nm.

of the mutants have substantial oxidase activity, at least 50% that of the wild-type, 1500 s^{-1}. R52A is essentially inactive, with approximately 0.5% of the wild-type activity. This small activity is most likely due to cbb_3-type cytochrome *c* oxidase contamination found in *R. sphaeroides* (*21*). Y414F is the next most inhibited mutant, with about 50% of the wild-type activity (*12*, *22*).

The electron-transfer rate of the oxidases reconstituted in phospholipid vesicles were all between 340 and 1000 e^-/s. All of the reconstituted oxidases (except the inactive R52A and R52Q mutants) demonstrated similar respiratory control ratios in the range of 4−6 (*12*) and showed similar proton-pumping stoichiometry as did the wild-type, about 0.2−0.5 proton/electron (data not shown).

The UV/vis spectra of the oxidized and reduced mutant enzymes are similar to those of the wild-type oxidase, with three notable exceptions: Q471A, Y414F, and R52A (Figure 3 and Table 2). Dithionite-reduced Q471A has its α-band blue-shifted by 4 nm (from 605 to 601 nm) and its Soret band blue shifted by 2.4 nm to 441.6 nm (from 444 nm in the wild-type oxidase). Reduced Y414F has its α-band red-shifted by 4.4 nm (from 605 to 609.4 nm) and its Soret band red-shifted by 1.4 nm. The α-band in dithionite-reduced R52A has a very large blue shift to 592.2 nm and also has a split Soret band with maxima at 421.4 and 438.4 nm. The split Soret is due to the fact that the R52A mutant is not fully reduced by dithionite under the conditions utilized, so heme a_3 remains partially oxidized. Clearly, the R52A mutant is the one most severely perturbed in the set examined. Two additional mutants were made at position R52, substituting glutamine (R52Q) and lysine (R52K). The R52Q mutant appears very similar to R52A and was not further analyzed. The R52K mutant retains most of the wild-type function but its α-band is red-shifted to 609 nm. All three residues (R52, Y414, and Q471) where mutants exhibited spectroscopic perturbation are in close proximity to the formyl group of heme *a* (Figure 4), the chromophore primarily responsible for the α-band absorbance (*23*).

Resonance Raman Spectra of R52K and R52A. The porphyrin in-plane vibrational modes in the high-frequency region (1300−1700 cm^{-1}) of the resonance Raman spectra of heme proteins are sensitive to the electron density in the

Table 2: Spectroscopic Data on Mutant and Wild-Type Oxidases[a]

R. sphaeroides residues	distance[b] to formyl oxygen atom [bovine/*P. denitrificans*]	α(reduced) (nm)	ν(C−O) reduced (cm^{-1})	ν(C−O) oxidized (cm^{-1})
WT		605.0	1611	1645
Q471A	3.9/3.6 Å	601.0	1628	1652
Y414F	-	609.4	1610	1650
R52K	3.2 for ω-N (3.8 for δ-N)/3.1 for δ-N (3.5 for ω-N)	609.0	1606	1640
R52A	3.2 for ω-N (3.8 for δ-N)/3.1 for δ-N (3.5 for ω-N)	592.2	1635	1638

[a] The samples were reduced with dithionite. X-ray crystal structure of bovine heart mitochondria oxidase (2OCC) and *Paracoccus denitrificans* (1AR1) was utilized with RASMOL to calculate distances. [b] Distance from formyl oxygen atom of heme *a* to the residue in wild-type X-ray structure, given in angstroms.

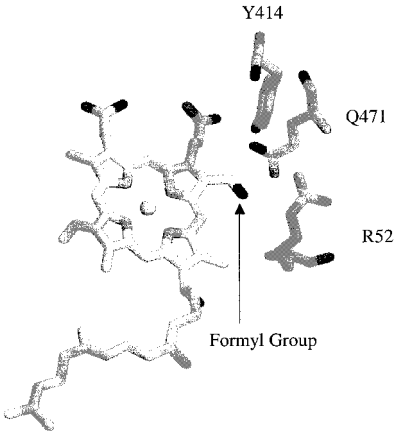

FIGURE 4: Proximity of Y414, Q471, and R52 (*R. sphaeroides* numbering) to heme *a*. Tyrosine 414 is near the electropositive side. Oxygen atoms are black and nitrogen atoms are darker gray. Hydrogen bonding distances are given in Table 2. The X-ray structure coordinates from *Paracoccus denitrificans* oxidase (1AR1) were used. This figure was prepared and the distances (Table 2) were calculated with RASMOL.

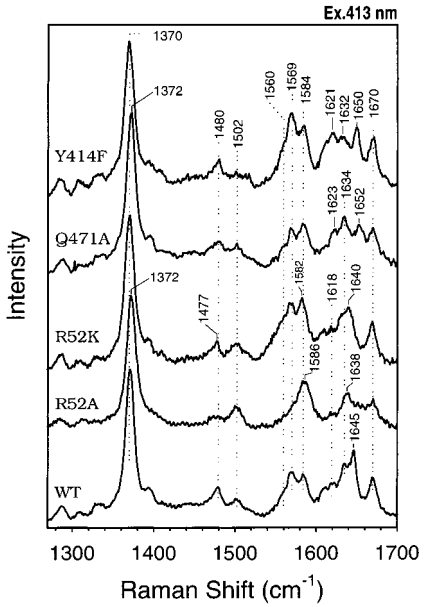

FIGURE 5: Resonance Raman spectra of R52K, R52A, Q471A, and Y414F of *R. sphaeroides* oxidized cytochrome *c* oxidase in the high-frequency region. The spectrum of the wild-type (WT) enzyme is also shown for comparison. The excitation wavelength is 413.1 nm. The laser power at the sample is ~2 mW. The mutant proteins are dissolved in 100 mM sodium phosphate buffer, pH 7.4, and 0.01% lauryl maltoside. It may be noted that the spectrum of the wild-type oxidized protein reported in an earlier paper (*36*) most likely contained some photoreduced protein that produced a relatively intense band at ~1613 cm^{-1}.

porphyrin macrocycle and to the oxidation, coordination, and spin states of the central iron atom (*24*). In the aa_3 oxidases, distinct Raman modes from hemes *a* and a_3 are observed that allow unambiguous identification of their spin, oxidation, and coordination states. In addition, the carbonyl stretching modes from the formyl groups on both heme *a* and heme a_3 (in the 1600−1680 cm^{-1} region) are resonance-enhanced and are useful probes of the conformation near the hemes.

The resonance Raman spectra of the as-isolated oxidized R52K and R52A mutants along with that of the wild-type enzyme are shown in Figure 5. The ν_4 marker line appears in the 1370−1372 cm^{-1} range, typical of ferric hemes, showing that both the hemes (*a* and a_3) are in the ferric state in both the mutant enzymes. The spectrum of the R52K mutant is very similar to that of the wild-type protein with small changes occurring in the 1630−1640 cm^{-1} region. In the ferric state of the wild-type protein, the low-spin heme *a* formyl stretching mode ($\nu_{C=O}$) is located at 1645 cm^{-1} and a porphyrin mode, ν_{10}, appears at about 1634 cm^{-1}. In the R52K mutant the $\nu_{C=O}$ of the heme *a* formyl group is shifted to 1640 cm^{-1} and broadened.

In contrast to the similarity in the spectra of R52K to the wild-type protein, the spectrum of the R52A mutant is significantly different (Table 2). There is a large increase in the intensity of the low-spin marker lines (ν_3 at 1502 cm^{-1}, ν_2 at 1586 cm^{-1}) with a corresponding decrease in the high-spin heme a_3 lines (ν_3 at 1477 cm^{-1}, ν_2 at 1569 cm^{-1}, $\nu_{C=O}$ at ~1669 cm^{-1}) and a significant change in intensity in the 1630−1640 cm^{-1} region. Thus, it appears that not only the environment around the heme *a* formyl group is changed but also the environment of heme a_3 has changed, resulting in a nearly complete conversion to a low-spin configuration. While the origin of the strong low-spin signal is puzzling, it should be noted that some of the low-spin signal may have arisen from a heme-containing impurity in this mutant that is detected in the hemochromogen assay (*25*). However, it is clear that the high-spin contribution to the spectrum is significantly reduced.

The resonance Raman spectra with excitation wavelengths of 413.1 and 441.6 nm of the reduced forms of R52K and R52A along with those of the wild-type enzyme for comparison are shown in Figure 6. In both mutants, the ν_4 line appears in the 1356−1358 cm^{-1} region, confirming that the hemes are in the ferrous oxidation state. In R52K, the heme a_3 lines are at frequencies similar to those in the wild-type enzyme. The marker lines of heme *a*, however, show significant differences in their frequencies (1513, 1581, and 1606 cm^{-1}) in comparison to those in the wild-type enzyme

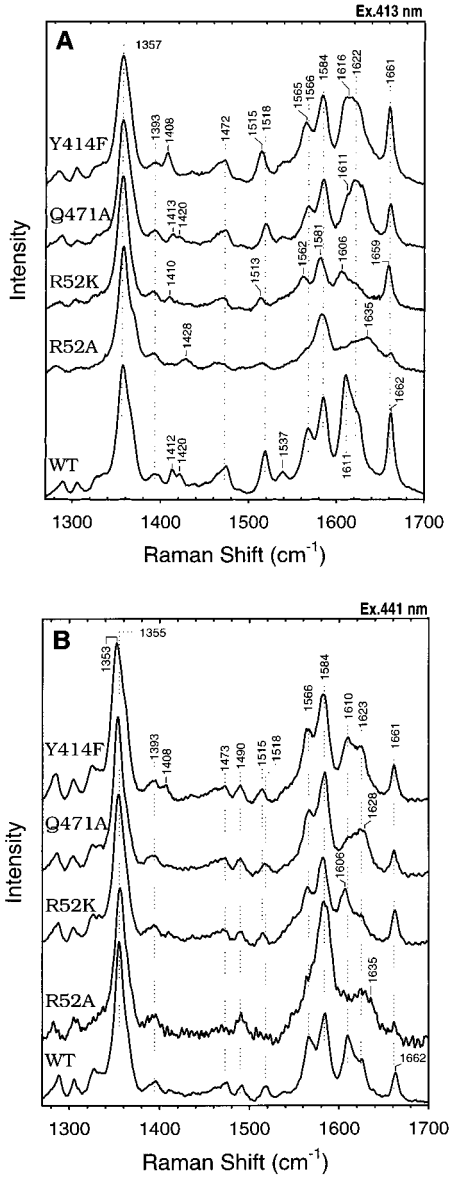

FIGURE 6: Resonance Raman spectra of R52K, R52A, Q471A, and Y414F mutants of *R. sphaeroides* dithionite-reduced cytochrome *c* oxidase in the high-frequency region. The spectrum of the wild-type (WT) enzyme is also shown for comparison. Excitation wavelengths are (A) 413.1 nm and (B) 441.6 nm. Laser power at the sample is ~10 mW. Sample conditions are the same as those in Figure 5.

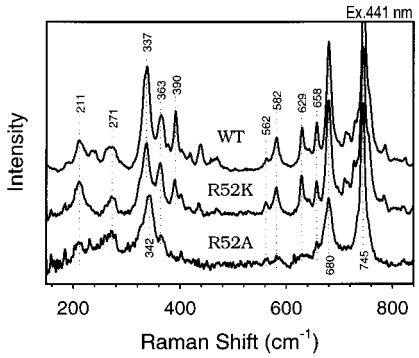

FIGURE 7: Resonance Raman spectra of R52K and R52A of *R. sphaeroides* dithionite-reduced cytochrome *c* oxidase in the low-frequency region. Excitation wavelength is 441.6 nm. Laser power at the sample is ~10 mW. Sample conditions are the same as those in Figure 5.

(1518, 1584, and 1611 cm^{-1}, respectively). Significantly, the $\nu_{C=O}$ mode of the formyl group of reduced heme *a* (at ~1611 cm^{-1} in the wild-type enzyme) shifts to lower frequency by 5 cm^{-1}, the same as the shift observed in ferric heme *a*. We attribute the lowering of the C−O stretching frequency of the formyl group to an increase in hydrogen-bonding strength between the inserted lysine residue at position 52 and the formyl of heme *a* (*26*, *27*). In the R52A mutant, no line is observed in the 1611 cm^{-1} region; instead, a new line appears at 1635 cm^{-1} that has a strong resemblance to the formyl $\nu_{C=O}$ mode in model heme *a* complexes in aqueous micellar medium, in which the $\nu_{C=O}$ frequency of low-spin heme *a* complex was assigned at 1634 cm^{-1} (*28*). Thus, in R52A, the environment of the heme *a* formyl group is very different from that in the wild-type enzyme. Replacement of the arginine by alanine at position 52 endows a micelle interior-like hydrophobic environment to the heme *a* formyl group. The stretching mode of the formyl group from heme a_3 is very weak in R52A, and the high-spin marker line at 1562 cm^{-1} is virtually absent, confirming that the environment around the binuclear center is also disrupted by this mutation. The disruption of the binuclear center in R52A is also seen in the low-frequency region of the resonance Raman spectrum with excitation at 441.6 nm (Figure 7). With this laser excitation wavelength, the Fe−histidine stretching mode (ν_{Fe-His}) for the high-spin, five-coordinate heme a_3 in the wild-type enzyme is detected. While the ν_{Fe-His} is clearly present at 211 cm^{-1} for R52K (similar as in the wild-type oxidase), it is very weak for R52A, which is consistent with a low-spin configuration of heme a_3. Thus, in R52K, the binuclear center is almost unperturbed by the effect of the mutation, but in R52A, the mutation has caused a significant structural change in the binuclear center.

Resonance Raman spectra of Q471A and Y414F. In the oxidized Q471A enzyme, the formyl group frequency of heme *a* is higher (1652 cm^{-1}) than that in the wild-type enzyme (1645 cm^{-1}) but the modes from heme a_3 appear at frequencies similar to those in the wild-type enzyme (Figure 5). Similarly, in the reduced enzyme, while the heme a_3 modes remain nearly unchanged, the heme *a* modes show appreciable changes that are apparent in the spectra obtained with both 413 and 441 nm excitation wavelengths (Figure 6). The heme *a* formyl mode at 1611 cm^{-1} has a much lower intensity than that in the wild-type enzyme. Furthermore, a new line appears at ~1628 cm^{-1} that is absent in the spectrum of the wild-type enzyme. The 1628 cm^{-1} line can be tentatively assigned to the frequency of heme *a* formyl mode with a significantly perturbed environment. The shift in frequency of the formyl mode of heme *a*, compared to the wild-type enzyme, is smaller in Q471A than in R52A but in the same direction.

The resonance Raman spectra of the reduced Y414F mutant are very similar to those of the wild-type enzyme with the exception of the intensity of the formyl mode of heme *a*, in agreement with earlier results (*22*). We find that, for both 413 and 441 nm excitation wavelengths, the intensity of the formyl stretching mode in the reduced mutant is weaker than that in the wild-type enzyme (Figure 6). However, in the oxidized form of Y414F (Figure 5), although most of the heme modes are unchanged, the heme *a* formyl mode shifts to higher frequency (1650 cm^{-1} versus 1645

cm^{-1} in the wild-type protein). The Y414 residue has no direct interaction with the formyl group; instead, it forms a hydrogen bond with one of the heme *a* propionate groups. Thus, the change in the formyl mode is attributed to a change in its local structure due to a change in the orientation of the nearby propionate group.

DISCUSSION

Functional Implications. The above results together with the previous studies with the oxidase from *P. denitrificans* (*29*) suggest that the putative H-channel is not functionally important for proton conduction in the bacterial oxidases. This is also suggested by the fact that most of the residues that line the walls of the putative H-channel in the mammalian oxidase are not highly conserved in the prokaryotic enzymes, as illustrated by the *E. coli* oxidase (Figure 2). The D51 residue (bovine numbering), near which interesting conformational changes (*9*) are observed upon reduction of the bovine oxidase, is absent in both *P. denitrificans* and *R. sphaeroides* oxidase sequences. All of the site-directed mutants along the length of the putative H-channel, with the exception of the R52A (discussed below), appear to have little or only modest influence on the specific activity of the enzyme, and no change in the efficiency of proton pumping upon mutation is observed. A similar conclusion resulted from the examination of the mutants in the oxidase from *P. denitrificans* (*29*). However, one difference from the previous results with the *P. denitrificans* oxidase (*29*) is that the mutation of residue H448 (corresponding to *R. sphaeroides* H456) resulted in a complete loss of activity as well as loss of heme *a*. In contrast, in the present work, the H456A mutant has properties comparable to those of the wild-type oxidase. The discrepancy can be rationalized by noting that the mutant examined in the *P. denitrificans* oxidase was a leucine substitution, and the larger hydrophobic side chain is likely responsible for greater structural disruption than the smaller alanine.

The equivalent of residue R52 in the *E. coli* cytochrome bo_3 oxidase has been mutated to a glutamine (R80Q) by Kawasaki et al. (*30*), and the enzyme was observed to lose the diagnostic peak for low-spin heme *b*. In cytochrome bo_3, the low-spin heme *b* is the counterpart of heme *a*. However, it is noteworthy that heme *b* does not have the formyl side chain, but instead has a methyl group at the same position of the porphyrin ring (*31*−*33*).

The results obtained with the prokaryotic oxidases concerning the putative H-channel strongly argue against a critical function for this channel, in contrast to the results obtained with the mutagenesis of the critical residues in both the D-channel and the K-channel (*8*). Several site-directed mutants that remove hydrogen-bonding capabilities of residues in the D- and K-channels result in major alterations in the proton pumping efficiency and/or the specific activity of the enzyme (*7*, *8*, *12*, *13*, *29*). The current data cannot rule out the possibility of a functional role for the H-channel in proton conduction in the eukaryotic oxidases, though it suggests otherwise. If the H-channel plays a critical role in the mammalian oxidase, then either the mechanism of proton pumping is different from that in the prokaryotic oxidases (*14*) or the role of the H-channel may be regulatory and without a corresponding prokaryotic function.

Spectroscopic Implications. The Q471A and R52A mutants cause a blue shift of the α-band to 601 and 592 nm, respectively. It has been reported in prior studies on model compounds that reduced low-spin heme *a* in an aqueous micellar medium has an absorption maximum near 597 nm, compared to 605 nm that is typical in cytochrome *c* oxidases (*28*). The spectrum of the R52A mutant, which should eliminate a hydrogen bond to the formyl group of heme *a*, seems to mimic the spectrum of free heme *a* (*28*). The same is observed for R52Q (not shown). The resulting reduced split Soret peak of the R52A mutant (and R52Q, as well) appears to be due to incomplete reduction of heme a_3, even in the presence of dithionite, consistent with perturbation of the heme a_3-Cu_B center.

Whereas for mutants R52A, R52K, Q471A, and Y414F, the α-band electronic transitions are all shifted in wavelength (Table 2), the direction of the spectroscopic shift is to shorter wavelengths for the mutants in R52A and Q471 but to longer wavelengths for the mutants Y414F and R52K. The C−O stretching modes of the formyl group of heme *a* in the resonance Raman spectrum display frequency shifts and intensity changes compared to the wild-type enzyme in the mutants of each of these residues. The residues R52, Q471, and Y414 are all located close to heme *a*. R52 and Q471 are hydrogen-bonded to the formyl group. The crystallographic distances for R52 are 3.1 Å for δ-N (3.5 Å for ω-N) and 3.2 Å for ω-N (3.8 Å δ-N) in the *P. denitrificans* (PDB code 1AR1) and bovine (PDB code 2OCC) structures, respectively; and for Q471 the distances are 3.9 and 3.6 Å, respectively. The hydroxyl of Y414 forms a hydrogen bond with the carboxylate group of one of the heme *a* propionates with crystallographic distances of 3.0 and 3.4 Å in the *P. denitrificans* (PDB code 1AR1) and bovine (PDB code 2OCC) structures, respectively. The origin of the shift in the α-band wavelength in Y414F is likely to be a perturbation in the structure near the formyl group resulting from a change in hydrogen bonding to the propionate. By releasing the hydrogen bonding to the propionate group, it is free to move, disrupting the native interactions of other residues with the formyl group. It is concluded that the changes in wavelength in the α-band electronic transition in the mutants of R52, Y414, and Q471 result from changes in the stereochemistry of the formyl group.

Although there are large changes in the environment near the formyl group of heme *a* for several of the mutants we have studied, only the R52A and R52Q mutants are inactive. All of the other mutants retain 50% or more of the wild-type activity. The spectroscopic data indicate that hydrogen bonding to the formyl group is maintained in the R52K mutant, where the polar arginine is replaced by the polar lysine. The hydrogen bond appears to be absent for both the R52A mutant as well as R52Q, even though the glutamine has the potential to form a hydrogen bond. We postulate that it is too short to reach the formyl oxygen atom and form a bond. However, the Q471A mutant is enzymatically active although the alanine substitution also disrupts the hydrogen bonding to the formyl group of heme *a*. Evidently, it is the absence of the positive charge at position 52 that correlates to the loss of enzymatic function. In addition to the changes in the environment near heme *a* in R52A and R52Q, there is a substantial perturbation of the structure of the binuclear center involving conversion of heme a_3 to a low-spin

configuration. Furthermore, these mutants were expressed in low yield and could not be purified to the same extent as the other mutants.

In addition to the absorption spectroscopic data, the resonance Raman results presented in the current work support the contention that the formyl group on heme *a* in cytochrome *c* oxidase is hydrogen-bonded to its neighboring groups. This hydrogen-bonding network causes the C−O stretching mode of the formyl group to be very low in frequency (∼1611 cm^{-1}) and modulates the position of the optical transition as postulated by Babcock et al. (*27*, *34*). It is noteworthy that, although strong hydrogen-bonding interactions cause the low frequency of the stretching mode of the formyl group, no model heme *a* complex, thus far, has been found to mimic the spectroscopy of the formyl group of reduced heme *a* in cytochrome *c* oxidase. The absence of hydrogen bonding with the heme *a* formyl (as in R52A), in fact, renders the heme *a* spectrum similar to that of heme *a* in an aqueous micelle (*28*). Finally, the notion that a stronger hydrogen bond results in a lower frequency of $\nu_{C=O}$ of the formyl, possibly due to enhanced electron delocalization into the −C═O π^*-orbital (*26*, *27*, *35*), is supported by the present work.

REFERENCES

1. Babcock, G. T., and Wikström, M. (1992) *Nature 356*, 301−309.
2. Ferguson-Miller, S., and Babcock, G. T. (1996) *Chem. Rev. 7*, 2889−2907.
3. Gennis, R. B., and Ferguson-Miller, S. (1996) *Curr. Biol. 6*, 36−38.
4. Trumpower, B. L., and Gennis, R. B. (1994) *Annu. Rev. Biochem. 63*, 675−716.
5. Iwata, S., Ostermeier, C., Ludwig, B., and Michel, H. (1995) *Nature 376*, 660−669.
6. Tsukihara, T., Aoyama, H., Yamashita, E., Takashi, T., Yamaguichi, H., Shinzawa-Itoh, K., Nakashima, R., Yaono, R., and Yoshikawa, S. (1996) *Science 272*, 1136−1144.
7. Wikström, M., Morgan, J. E., and Verkhovsky, M. I. (1998) *J. Bioenerg. Biomembr. 30*, 139−145.
8. Gennis, R. B. (1998) *Biochim. Biophys. Acta 1365*, 241−248.
9. Yoshikawa, S., Shinzawa-Itoh, K., Nakashima, R., Yaono, R., Yamashita, E., Inoue, N., Yao, M., Fei, M. J., Libeu, C. P., Mizushima, T., Yamaguchi, H., Tomizaki, T., and Tsukihara, T. (1998) *Science 280*, 1723−1729.
10. Ostermeier, C., Harrenga, A., Ermler, U., and Michel, H. (1997) *Proc. Natl. Acad. Sci. U.S.A. 94*, 10547−10553.
11. Thomas, J. W., Puustinen, A., Alben, J. O., Gennis, R. B., and Wikström, M. (1993) *Biochemistry 32*, 10923−10928.
12. Fetter, J. R., Qian, J., Shapleigh, J., Thomas, J. W., Garcia-Horsman, A., Schmidt, E., Hosler, J., Babcock, G. T., Gennis, R. B., and Ferguson-Miller, S. (1995) *Proc. Natl. Acad. Sci. U.S.A. 92*, 1604−1608.
13. Hosler, J. P., Shapleigh, J. P., Mitchell, D. M., Kim, Y., Pressler, M., Georgiou, C., Babcock, G. T., Alben, J. O., Ferguson-Miller, S., and Gennis, R. B. (1996) *Biochemistry 35*, 10776−10783.
14. Gennis, R. B. (1998) *Science 280*, 1712−1729.
15. Vandeyar, M. A., Weiner, M. P., Hutton, C. J., and Batt, C. A. (1988) *Gene 65*, 129−133.
16. Landt, O., Grunert, H.-P., and Hahn, U. (1990) *Gene 96*, 125−128.
17. Mitchell, D. M., and Gennis, R. B. (1995) *FEBS Lett. 368*, 148−150.
18. Hosler, J. P., Fetter, J., Tecklenberg, M. M. J., Espe, M., Lerma, C., and Ferguson-Miller, S. (1992) *J. Biol. Chem. 267*, 24264−24272.
19. Puustinen, A., Finel, M., Virkki, M., and Wikström, M. (1989) *FEBS Lett. 249*, 163−167.
20. Puustinen, A., Finel, M., Haltia, T., Gennis, R. B., and Wikström, M. (1991) *Biochemistry 30*, 3936−3942.
21. Garcia-Horsman, J. A., Berry, E., Shapleigh, J. P., Alben, J. O., and Gennis, R. B. (1994) *Biochemistry 33*, 3113−3119.
22. Hosler, J. P., Shapleigh, J. P., Tecklenburg, M. M. J., Thomas, J. W., Kim, Y., Espe, M., Fetter, J., Babcock, G. T., Alben, J. O., Gennis, R. B., and Ferguson-Miller, S. (1994) *Biochemistry 33*, 1194−1201.
23. Vanneste, W. H. (1966) *Biochemistry 65*, 838−848.
24. Argade, P. V., Ching, Y. C., and Rousseau, D. L. (1986) *Biophys. J. 50*, 613−620.
25. Berry, E. A., and Trumpower, B. L. (1987) *Anal. Biochem. 161*, 1−15.
26. Das, T. K., Gomes, C. M., Teixeira, M., and Rousseau, D. L. (1999) *Proc. Natl. Acad. Sci. U.S.A. 96*, 9591−9596.
27. Babcock, G. T., and Callahan, P. M. (1983) *Biochemistry 22*, 2314−2319.
28. Han, S., Ching, Y.-c., Hammes, S. L., and Rousseau, D. L. (1991) *Biophys. J. 60*, 45−52.
29. Pfitzner, U., Odenwald, A., Ostermann, T., Weingard, L., Ludwig, B., and Richter, O.-M. H. (1998) *J. Biomembr. Bioenerg. 30*, 89−93.
30. Kawasaki, M., Mogi, T., and Anraku, Y. (1997) *J. Biochem. (Tokyo) 122*, 422−429.
31. Puustinen, A., Morgan, J. E., Verkhovsky, M., Thomas, J. W., Gennis, R. B., and Wikström, M. (1992) *Biochemistry 31*, 10363−10369.
32. Puustinen, A., and Wikström, M. (1991) *Proc. Natl. Acad. Sci. U.S.A. 88*, 6122−6126.
33. Wu, W., Chang, C. K., Varotsis, C., Babcock, G. T., Puustinen, A., and Wikström, M. (1992) *J. Am. Chem. Soc. 114*, 1182−1187.
34. Callahan, P. M., and Babcock, G. T. (1983) *Biochemistry 22*, 452−461.
35. Choi, S., Lee, J. J., Wei, Y. H., and Spiro, T. G. (1983) *J. Am. Chem. Soc. 105*, 3692−3707.
36. Das, T. K., Pecoraro, C., Tomson, F. L., Gennis, R. B., and Rousseau, D. L. (1998) *Biochemistry 37*, 14471−14476.

BI9924821